Original article

Modeling the elastic characteristics of overpressure due to thermal maturation in organic shales

Xuan Qin[1]◉*, Luanxiao Zhao[2]◉*, Jinwan Zhu[2], De-hua Han[1]

[1]*Department of Earth and Atmospheric Sciences, University of Houston, Houston 77004, USA*
[2]*State Key Laboratory of Marine Geology, Tongji University, Shanghai 200092, P. R. China*

Abstract:
Modeling the overpressure of organic shales caused by thermal maturation and its elastic responses is crucial for geophysical characterization of source rocks and unconventional shale reservoirs. Thermal maturation involves the generation of excess fluid contents (oil and gas) and can cause the overpressure if an organic shale preserves the produced fluids partly or wholly. The solid organic matter (e.g., kerogen or solid bitumen) with the potential of generating hydrocarbon presents two types of morphology in organic shales: scattered patches as pore-fillings and continuous network as load-bearings. According to the kerogen morphology, two bulk volume models are devised to simulate the elasticity of organic shales using respective rock-physics modeling schemes. The rock physics modeling combined with the density and compressibility of pore-fillings are demonstrated to effectively capture the excess pore pressure characteristics due to thermal maturation in organic shales. The basic principle of solving the overpressure is that the pore space volume equals the total volume of all components within the pores before and after the maturation. According to the modeling results, the elastic characteristics of overpressure due to thermal maturation reveal a decrease in velocity and a slight decrease in density. Besides, for an organic shale with a relatively rigid framework, it tends to yield higher overpressure than a shale with a relatively compliant framework. With proper calibration, the modeling strategy shows its potential in quantitatively interpreting the well-log data of organic shale formation within the thermal maturation window.

1. Introduction

Although numerous scholars investigated pore-pressure prediction in shale, most studies focus on the mechanism of the disequilibrium compaction (Hart et al., 1995; Gutierrez et al., 2006; Sayers, 2006; Zhang, 2011; Yu, 2015), which forms during the burial process. In recent years, organic shales have attracted more attention because they are more than hydrocarbon source rocks and can produce oil and gas as unconventional reservoirs with proper stimulation. Knowledge of pore pressure can ensure the safety of drilling activity, such as preventing breakouts (Swarbrick and Osborne, 1998; Chatterjee et al., 2011) and maintaining borehole stability (Zou et al., 2017). Also, studying pore pressure in organic shale can identify the type and accumulation status of pore fluids

(Bruce, 1984; Hao et al., 2007). In particular, the overpressure signatures of organic shale are closely associated with the identification of sweet spots in unconventional reservoirs. For instance, Karthikeyan et al. (2018) found that excess pore pressure positively correlates with production in the Marcellus Shale gas reservoir.

Kerogen, in the form of amorphous organic matter (OM), possesses the capability of generating hydrocarbon when heated under in-situ conditions. Thermal maturation of kerogen or hydrocarbon generation takes place through a series of decomposition reactions (Luo and Vasseur, 1996; Carcione and Gangi, 2000), and the OM maturation can primarily be divided into three stages (Tissot et al., 1987; Barker, 1990; Vernik and Landis, 1996; Seewald, 2003; Passey et al., 2010). At the immature stage, the historical maximum formation

temperature is lower than 50 °C, and kerogen has a vitrinite reflectance (R_o), of less than 0.5%. Kerogen does not decompose to generate thermogenic hydrocarbon. The organic-rich shale (oil shale) can be treated as a type of fuel resource. At the mature stage, when the formation temperature is between 60 and 150 °C, generative kerogen decomposes to generate oil as the primary product. Vitrinite reflectance of $0.5 < R_o(\%) <$ 1.1-1.3 marks the window of oil generation. The preserved oil or condensate in organic shales composes "shale oil". At the overmature stage, $R_o(\%) > 1.1 - 1.3$, gas is the main product of a secondary cracking of oil or organic residues.

The thermal maturation process of kerogen can result in overpressure. First, the reaction of phase transition resembles a process of volume expansion of pore fluids because the products of OM maturation have smaller densities than kerogen. For instance, kerogen or solid bitumen has a density varying from 1.1 to 1.4 g/cm^3, oil's density usually varies from 0.75 to 0.95 g/cm^3, and gas density ranges from 0.01 to 0.2 g/cm^3. Meissner (1978) suggested the volume expansion could be as high as 25% during kerogen transforming to oil, gas, and other byproducts. Second, the generated hydrocarbon is difficult to percolate or migrate out of the low-permeability organic shales, so the hydrocarbon keeps accumulating and increasing the pore pressure (Bowers, 1995; Carcione and Gangi, 2000; Ramdhan and Goulty, 2011; Tingay et al., 2013) until surpassing the fracturing pressure (Zhang et al., 2022). After a part of the hydrocarbon is expelled from fractures, formed pathways remain closed, and the organic shale repeats the process of hydrocarbon generation, accumulation, and expulsion. Luo and Vasseur (1996) and Swarbrick et al. (2001) estimated the overpressure magnitude through basin modeling and suggested that the gas generation stage produced higher pressure than the oil generation stage. The gas generation was considered to generate local high-magnitude pore pressure (Morley, 1992; Burrus et al., 1996; Lash and Engelder, 2005) until Tingay et al. (2013) reported the basin-scale overpressure due to the gas generation in the Malay Basin.

Geoscientists and engineers modified conventional methods to interpret the geophysical properties variation and predict pore pressure in organic shales containing thermal maturation. These methods include increasing the Eaton exponent from 3 to over 10 (Eaton, 1975; Bowers, 1995; Tingay et al., 2013; Dasgupta et al., 2016) and elastic unloading method by Bowers (1995). Some authors have analyzed and estimated overpressure in unconventional shales. Couzens-Schultz et al. (2013) suggested combing a constant vertical effective stress of offset wells with the information of erosion or burial while predicting pore pressure in various unconventional plays. Green et al. (2018) proposed a pressure reference trend to modify the traditional pore-pressure prediction techniques in a gas shale play that experienced tectonic uplift or erosion. Therefore, both the complex tectonic history (an external source of unloading/reloading) and OM conversion influence the pore-pressure evolution as well as its geophysical properties in unconventional shales. These make the derivation of a normal compaction trend (NCT) with porosity proxies (sonic velocity, density, or resistivity) yield uncertainties in the pore-pressure prediction for unconventional shales. Consequently,

the aim is to develop a theoretical method to offer insights into decoupling the multiple factors affecting the pore-pressure prediction in organic shales, and hopefully discerning the unique elastic characteristics of overpressure due to thermal maturation.

Thermal maturation alters the fabric and texture of organic shales. For instance, the porosity and morphology of OM pore evolve during the maturation (Loucks et al., 2009; Walls and Diaz, 2011; Modica and Lapierre, 2012; Milliken et al., 2013; Chen and Xiao, 2014). In highly mature samples, microcracks can be observed from the scanning electron microscopy (Berg and Gangi, 1999; Lash and Engelder, 2005; Jarvie et al., 2007), which is consistent with the increasing pressure sensitivity of ultrasonic velocity or velocity anisotropy in rock-physics measurements (Vernik, 1994; Vanorio et al., 2008). Therefore, as the presence and the maturation process of kerogen complicate the physical properties of organic shales (Vernik and Landis, 1996; Zhao et al., 2018, 2023; Qin et al., 2022), a few authors consider the role of kerogen at different maturation stages in their modeling work. Qin et al. (2014) and Zhao et al. (2016) modeled the effects of kerogen maturation on the elastic stiffness of organic shale based on the analysis of the composition and microstructure of organic shales. Yang and Mavko (2018) modeled the crack growth due to kerogen maturation and the concomitant overpressure at the laboratory and geological conditions. However, the thermal maturation simultaneously impacts the evolution of elasticity of organic shales and the generation of overpressure, which are lack of systematical investigation.

Through a modeling framework, this paper primarily focuses on establishing the link between pore pressure evolution and elastic properties in organic shales under the effects of kerogen thermal maturation. The structure of the paper is organized as follows: First, based on the role of OM, acting as a part of pore-filling or load-bearing, different bulk volume models and rock physics modeling strategies are adopted. Then, the pore pressure increase due to thermal maturation is solved with the linear poroelastic theory. Subsequently, the modeling results, especially the effect of pore pressure evolution on the elastic characteristics, are analyzed. Finally, the modeling workflow is employed to interpret a well-log data set, offering insights into the elastic signatures of overpressure caused by thermal maturation.

2. OM morphology in organic shale

Organic shales comprise inorganic minerals and solid OM (kerogen, solid-bitumen, or pyro-bitumen) along with pore space within and between these particles. The pore space can be divided into two parts in unfractured rocks: the mineral pore and OM pore. The mineral porosity decreases from a critical porosity (Nur et al., 1998) to a few percent (e.g., 1%) with continual burial due to the impacts of compaction. The OM pore forms due to the thermal decomposition of kerogen, and the kerogen-related porosity enlarges with the increase in depth (Cander, 2012; Modica and Lapierre, 2012; Dong et al., 2019).

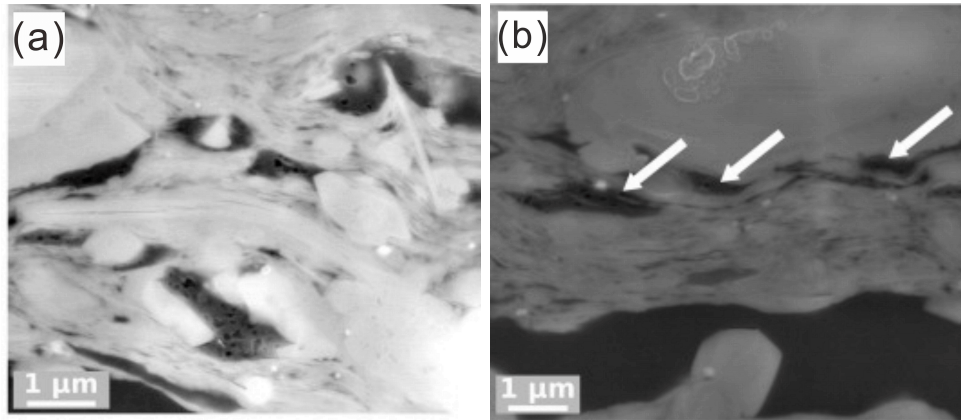Continuous laminae and dispersed spheroids are two typ-

Fig. 1. Scanning electron microscopy images of the overmature Woodford shale (Löhr et al., 2015): (a) round pores exist in dispersed OM bodies and (b) no pores exist in the larger domains of OM in a laminar shape, while only smaller domains of OM are porous (marked by white arrows). The minerals, organic bodies, and pores are respectively in bright, gray, and black colors.
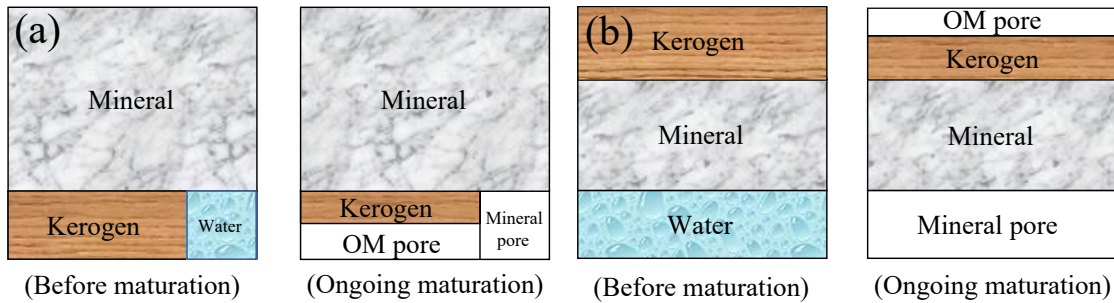

Fig. 2. Bulk volume models of organic shales when (a) OM is a part of pore-filling components and (b) OM is a part of load-bearing.

ical phases of kerogen, as shown in Fig. 1. A Woodford overmature shale (Löhr et al., 2015) is in the gas window with a R_o at 1.5% and total organic carbon (TOC) at 6.2%. The minerals, organic bodies, and pores are respectively in bright, gray, and black colors. In Fig. 1(a), rounded pores in dispersed organic bodies are observed, filled in the inorganic matrix. In Fig. 1(b), the larger domains in a laminar shape are non-porous and appear homogeneous, while only smaller domains of OM are porous (marked by white arrows). If the yielded OM pores have been compacted within the larger domain, the laminar OM directly supports the load-bearing. The intraparticle or secondary OM pores within the smaller domains of OM do not collapse even in stress-bearing conditions. They tend to be preserved at locations where the presence of sheltering rigid framework hinders the compaction of dispersed organic bodies. Therefore, the porous kerogen can be treated as a pore-filling component as other fluids within the rock matrix.

3. Modeling workflows

A bulk volume model is described to capture the elastic responses of organic shales, and the overpressure is estimated based on the link between the evolution of poroelastic characteristics of organic shales and pore fluids due to kerogen maturation.

3.1 Bulk volume model

Organic shales consist of inorganic minerals (mainly clay, quartz-feldspar, and carbonates), solid OM (kerogen as the primary component in low-maturity stages and pyro-bitumen as the chief organic residue in the overmature stage), and pore fluids (water and hydrocarbon). As shown in Fig. 2, an organic shale is composed of a kerogen part (V_k) and a non-kerogen part (V_{nk}), regardless of what role kerogen is, a part of pore-fillings (Fig. 2(a)) or load-bearing (Fig. 2(b)). The kerogen part consists of solid OM and OM pores, while the non-kerogen part comprises inorganic minerals and mineral pores (Alfred and Vernik, 2012; Milliken et al., 2013). Therefore, the volume fraction of voids ($\phi_t = \phi_k + \phi_{nk}$) equals the sum of kerogen-related porosity (ϕ_k) and non-kerogen-related porosity (ϕ_{nk}). The solid density ρ_m is expressed as:

$$\rho_m = v_{os}\rho_k + (1 - v_{os})\rho_{nk} \qquad (1)$$

where v_{os} is the volume fraction of the solid OM in the solid phase, and ρ_k and ρ_{nk} are the densities of the solid OM and inorganic minerals.

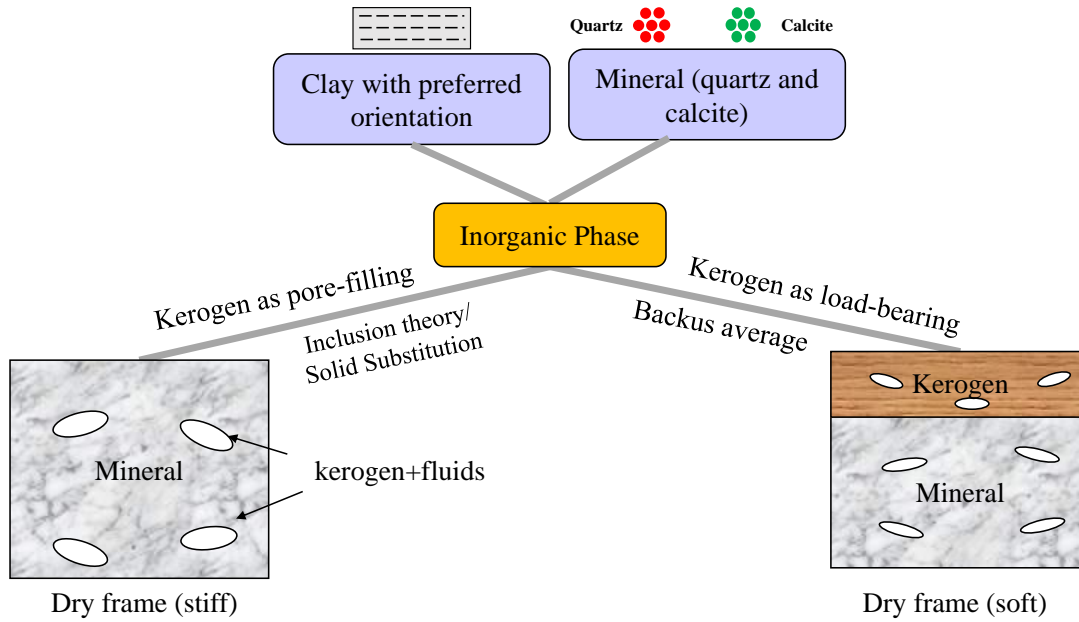The volume fraction of solid OM in the matrix v_{os} relates

Fig. 3. Schematic of rock-physics modeling in organic shale with kerogen serving as a part of pore-filling or a part of load-bearing.

to through:

$$\text{TOC} = v_{os} W_{om} \frac{\rho_k}{\rho_m} \qquad (2)$$

where W_{om} represents the carbon weight fraction in OM, usually ranging from 0.7 to 0.85 with increasing maturity (Vernik and Milovac, 2011), and thus, v_{os} or TOC does not depend on the pore fluids. By substituting Eq. (1) into Eq. (2), the volume fraction of solid organic matter is expressed as:

$$v_{os} = \text{TOC} \frac{\rho_{nk}}{W_{om}\rho_k + \text{TOC}(\rho_{nk} - \rho_k)} \qquad (3)$$

so that the TOC value can be estimated by given densities of the solid OM and inorganic minerals.

The relationship among volume fractions of the OM pore, minerals, and solid OM in the bulk rock will be explicitly defined. For a particular type of kerogen, the lability (N) of organic carbon is found experimentally correlated to the incipient hydrogen index (HI, in units of mg HC/g TOC) (Daly and Edman, 1987; Modica and Lapierre, 2012), i.e., $N(\%) = 0.085 \times \text{HI}$. When the formation temperature is heated above 50 °C, kerogen becomes thermally unstable and starts to decompose to generate hydrocarbons such as oil and gas and leave voids as OM pores. If kerogen bodies are spherical or dispersed as pore-fillings, the OM pores remain open after the decomposition of kerogen due to the stiff rock frame. By combining the lability (N) and a thermal transformation ratio of kerogen (F), the kerogen-related porosity satisfies:

$$\phi_k = (1 - \phi_{nk})NF v_{ik} \qquad (4)$$

where v_{ik} represents the initial value of the solid OM volume fraction in the solid part of an organic shale. The above formula does not consider the impact of pressure on pore space. The volume fractions of minerals f_{mi} and solid OM

f_{om} are expressed as:

$$f_{mi} = \frac{(1 - \phi_{nk})(1 - v_{ik})}{V_T} \qquad (5)$$

$$f_{om} = \frac{(1 - \phi_{nk})(1 - NF)v_{ik}}{V_T} \qquad (6)$$

where V_T denote the bulk volume and can be set as 1.

3.2 Modeling the elastic stiffness

After introducing the bulk volume model, two corresponding strategies are applied in Fig. 3 to theoretically model the stiffness of organic shale. The main question to answer is what kind of effective medium theories can be chosen to simulate the equivalent elasticity of organic shale.

3.2.1 Modeling the elasticity of inorganic solid phase

First, the stiffness of the inorganic solid phase is modeled, whose primary constituents include clay, quartz, and carbonate. Clay platelets are treated as a transverse isotropic (TI) material (Tosaya, 1982; Sayers, 1994) and have five elastic constants. For instance, C_{11} = 65 GPa, C_{33} = 52.7 GPa, C_{44} = 21.9 GPa, C_{66} = 25.8 GPa, and C_{13} = 38.5 GPa for illite (Carcione et al., 2011) or C_{11} = 44.9 GPa, C_{33} = 24.2 GPa, C_{44} = 3.7 GPa, C_{66} = 11.6 GPa, and C_{13} = 18.1 GPa for clay mineral particles containing the effect of clay bound water (Sayers, 2012). Quartz and carbonate are treated as isotropic materials, e.g., the bulk and shear moduli are 37 and 44 GPa for quartz and 77 and 32 GPa for calcite (Mavko et al., 2009). As minerals can be sourced from detrital, authigenic, or biogenic provenance (Hart et al., 2013), they can play different roles in shales: load-bearing of the framework, cement between the grains (quartz or calcite), or pore-filling that usually does not stiffen the frame. For our convenience,

the Self-Consistent Approximation in the anisotropic domain (Hornby et al., 1994) is employed to generate the stiffness of inorganic solid phase because it does not identify a specific type of mineral as the host material. The equivalent stiffness of the inorganic solid is calculated by iteratively merging all components:

$$\sum_{r=1}^{R} v_r \left(C^r - C^{sl} \right) \left[1 + \widehat{G} \left(C^r - C^{sl} \right) \right] = 0 \qquad (7)$$

where r represents the number of phase; R represents the sum of the number of phases; v_r represents the volume fraction of the r-th component for the inorganic solid phase; C^r denotes the stiffness tensor of the r-th component; C^{sl} represents the effective stiffness tensor of the inorganic solid phase; and $\widehat{G}$ is a fourth-rank tensor given by integrating the strain Green's function over the inclusion shape (Mura, 1987). In our modeling, quartz and carbonate have a spherical shape and clay has an elongated shape and aspect ratios are used to parameterize their geometry.

3.2.2 Modeling the elastic response of an organic shale

Then, shale is modeled as a porous medium, and the organic phase is included. If kerogen is dispersed, kerogen is treated as a type of pore-filling. Pores with zero moduli are added into the inorganic background to simulate the elasticity of the drained frame using the Differential Effective Medium (DEM) method in the anisotropic domain (Nishizawa, 1982; Hornby et al., 1994). This algorithm adds a small number of inclusions incrementally to a background host medium until a desired concentration of the inclusion is achieved:

$$\frac{d}{dv} \left(C^{fr}(v) \right) = \frac{C^0 - C^{fr}(v)}{(1-v) \left[I + \widehat{G}(C^0 - C^{fr}(v)) \right]} \qquad (8)$$

where $C^{fr}(v)$ represents the stiffness tensor of the drained frame containing pores with zero moduli at a volume fraction of v, and C^0 indicates the stiffness tensor of the inorganic mineral mixture, I is the unit tensor for tensors of fourth rank. Here the pore space volume equals the total volume of initial kerogen volume and mineral pore volume; the pore aspect ratio is set as 0.1, which simulates the geometry of interparticle pores in shales. When seismic waves propagate in organic shales, due to the low mobility (the permeability of the rock divided by the fluid viscosity), the mixtures of pore-fillings rarely satisfy the iso-stress condition, i.e., the mixtures of kerogen, generated oil, and water are not uniformly distributed and are therefore considered as a patch mixing. Thus, the equivalent bulk (K) and shear (G) moduli of the pore-filling are computed via the Voigt average (Domenico, 1976; Mavko et al., 2009):

$$K_{pf} = K_{om} \frac{V_{om}}{\phi_t} + K_w \frac{\phi_{nk}}{\phi_t} + K_o \frac{\phi_k}{\phi_t}$$
$$G_{pf} = G_{om} \frac{V_{om}}{\phi_t} \qquad (9)$$

where the volume fractions of kerogen, water, and oil are normalized by the total porosity (the sum of the volume fractions of original kerogen and mineral pores or $\phi_t = V_k + \phi_{nk}$), and

subscripts "pf", "om", "w", and "o" represent pore-fillings, solid OM, water, and oil. At last, the solid substitution equation (Ciz and Shapiro, 2007) is used to add the mixture of pore-fillings into the drained frame to capture the comprehensive responses of organic shales:

$$S_{ijkl}^{sa} = S_{ijkl}^{fr} - \frac{\left(S_{ijkl}^{fr} - S_{ijkl}^{sl} \right) - \left(S_{mnpq}^{fr} - S_{mnpq}^{sl} \right)}{[(S^{fr} - S^{solid}) + \phi_t (S^{pf} - S^{\phi})]_{mnpq}} \qquad (10)$$

where S_{ijkl}^{sa}, S^{fr}, S^{sl}, S^{pf}, and S^{ϕ} are the fourth-rank compliance tensors for the organic shale, drained frame, inorganic solid phase, mixtures of pore-fillings, and pore space. For simplicity, S^{ϕ} is assumed to be identical to S_{ijkl}^{sl} as the homogeneous condition.

Alternatively, if kerogen is distributed in a lenticular manner, kerogen serves as a part of load-bearing along with other minerals. Backus average (Backus, 1962) is employed to constitute a layered medium composed of organic and inorganic phases. The Backus average in a TI medium can be expressed as:

$$C_{11}^* = \frac{\left\langle \dfrac{C_{13}}{C_{33}} \right\rangle^2}{\left\langle \dfrac{1}{C_{33}} \right\rangle} - \left\langle \dfrac{C_{13}^2}{C_{33}} \right\rangle + \langle C_{11} \rangle$$

$$C_{33}^* = \left\langle \dfrac{1}{C_{33}} \right\rangle^{-1}$$

$$C_{13}^* = \frac{\left\langle \dfrac{C_{13}}{C_{33}} \right\rangle}{\left\langle \dfrac{1}{C_{33}} \right\rangle} \qquad (11)$$

$$C_{44}^* = \left\langle \dfrac{1}{C_{44}} \right\rangle^{-1}$$

$$C_{66}^* = \langle C_{66} \rangle$$

where $\langle \rangle$ indicates the arithmetic average of the enclosed properties weighted by their volumetric fractions. As an example, $\langle C_{11} \rangle = (f_{mi} + \phi_{nk}) C_{11}^{nk} + (f_{om} + \phi_k) C_{11}^k$, where the first and second terms denote the weighted C_{11} for the non-kerogen part and kerogen part. The mineral pores are assumed to be water-saturated, so the elasticity of the non-kerogen part can be modeled by adding water-filled pores into the inorganic background with DEM in the anisotropic domain (Nishizawa, 1982). The DEM algorithm yields a high-frequency result, which is representative of the seismic response in organic shales due to the unrelaxed pore pressure caused by the wave oscillation. The OM pores are assumed to be saturated with hydrocarbon, so the equivalent stiffness of hydrocarbon-saturated kerogen (kerogen part) can be modeled by adding hydrocarbon-filled pores into the solid OM with Self-Consistent Approximation (Berryman, 1980).

3.3 Estimating overpressure

The thermal cracking process of kerogen to hydrocarbon under constant confining pressure (P_c) leads to a decrease in the volume of solid material and an increase in the volume of fluid. The original space occupied by the decomposed

kerogen is replaced by the generated fluid and continues to resist the confining pressure. Thus, pore fluids support an increasing proportion of confining pressure than before, and the overpressure occurs. Because the density of produced hydrocarbon (generally < 1 g/cm^3) is less than solid OM (1.1-1.4 g/cm^3) (Alfred and Vernik, 2012), the increase in pore fluid volume is more substantial than the increase of pore space. The overpressure or pore pressure increase can be solved by accommodating all the pore-fillings in the pore space.

3.3.1 Kerogen as a part of pore-filling

If kerogen exists as a pore-filling, the OM pores remain open because the shale framework is stiff, and the pore compressibility is low. Fig. 4(a) schematically illustrates the evolution of volumes of pore-fillings and pore space. Increasing pore pressure can increase the volume of pore space but decrease the volumes of pore-fillings, so the pore pressure is raised to attain a new balance through accommodating the pore-fillings in the pore space. Before the kerogen maturation, the total volume of pore-fillings is identical to the volume sum of the kerogen part and mineral pore, $V_k + \phi_{nk}V_T$, where the bulk volume of the rock (V_T) is set as unity for convenience. The initial pore water volume (V_{wi}) equals the mineral pore space at the initial pore pressure, P_0. During the maturation, kerogen, hydrocarbon, and water occupy the pore space as pore-fillings, and an iso-stress condition is assumed for the pore fillings. Thus, a pore pressure increase (ΔP) is expected to accommodate all the pore-fillings in the pore space. The volume of the pore space equals the volume of all pore-fillings, so there is:

$$(V_k + \phi_{nk})(1 + \beta_{pp}\Delta P) = (1 - NF)V_k(1 - C_{om}\Delta P) \\ + V_{wi}(1 - C_w\Delta P) + V_{HC}(1 - C_{HC}\Delta P) \tag{12}$$

where $V_k + \phi_{nk}$, $(1 - NF)V_k$, V_{wi}, and V_{HC} represent the volume of pore space, remained solid OM, water, and hydrocarbon before the pressure gets equilibrium. V_k is volumes of void space filled by solid OM. β_{pp} is a poroelastic parameter indicating the pore compressibility upon solely pore pressure change; C_{om}, C_w, and C_{HC} denote the compressibility for the solid OM, water, and hydrocarbon. By definition, it is stated:

$$\beta_{pp} = +\frac{1}{V_p}\frac{\partial V_p}{\partial P}\bigg|_{P_c} \tag{13}$$

$$C_{om,w,hc} = -\frac{1}{V_{om,w,hc}}\frac{\partial V_{om,w,hc}}{\partial P} \tag{14}$$

Hereby a positive volumetric strain represents "extension" and thus "+" and "−" signs represent extension and compression, respectively. According to the mass balance, the assumption is that the mass of hydrocarbon equals the mass of decomposed kerogen. Therefore, the volume of hydrocarbon (V_{HC}) in the rock is a function of the lability of organic carbon (N), transformation ratio of kerogen (F), and expulsion/leakage ratio of hydrocarbon (E) through:

$$V_{HC} = (1 - E)NFV_k\frac{\rho_k}{\rho_{HC}} \tag{15}$$

If the density and compressibility of solid OM (ρ_k), water, and hydrocarbon (ρ_{HC}) are irrelevant with pressure, Eq.

(12) can be solved analytically:

$$\Delta P = \\ \frac{\left[(1 - E)\frac{\rho_k}{\rho_{HC}} - 1\right]NF}{\left(\frac{\phi_{nk}}{V_k} + 1\right)\beta_{pp} + (1 - NF)C_{om} + \frac{\phi_{nk}}{V_k}C_w + (1 - E)NF\frac{\rho_k}{\rho_{HC}}C_{HC}} \tag{16}$$

According to the expression of pore pressure increase (Eq. (16)), the decrease in the ratio of ϕ_{nk} to V_k can enhance the peak pore pressure, which means the smaller the non-kerogen-related porosity, the readier to accumulate a high pore pressure.

3.3.2 Kerogen as a part of load-bearing

If kerogen is a part of load-bearing, pore-fillings comprise water and hydrocarbon during the thermal maturation. For this scenario, the pore compressibility is only associated with the void space filled by fluids. Also, considering the solid OM has the same order of compressibility as water (Yan and Han, 2013), so the increased pore pressure will compress the solid OM to increase pore space. As shown in Fig. 4(b), to satisfy the criteria of pore space volume equaling the total volume of pore fluids, the following relationship holds:

$$V_\phi(1 + \beta_{pp}\Delta P) + V_kC_{om}\Delta P \\ = V_{wi}(1 - C_w\Delta P) + V_{HC}(1 - C_{HC}\Delta P) \tag{17}$$

where V_ϕ is volumes of void space filled by fluids. These volumes can be expressed as:

$$V_\phi = V_T(\phi_k + \phi_{nk}) \tag{18}$$

$$V_k = (1 - \phi_{nk})v_{ik}(1 - NF) \tag{19}$$

$$V_{wi} = \phi_{nk} \tag{20}$$

The pore pressure increase can be expressed as:

$$\Delta P = \frac{V_{wi} + V_{HC} - V_\phi}{V_\phi\beta_{pp} + V_kC_{om} + V_{wi}C_w + V_{HC}C_{HC}} \tag{21}$$

In both cases, the pore compressibility upon pore pressure change is utilized. The pore compressibility upon pore pressure change can be calculated with the bulk moduli of the solid phase (K_0), drained frame modulus (K_{fr}), and porosity ϕ by neglecting the heterogeneity of the inorganic mineral (Zimmerman, 1991):

$$\beta_{pp} = \left(\frac{\frac{1}{K_{fr}} - 1 - \phi}{\phi K_0}\right) \tag{22}$$

Because the drained rock frame and the solid phase are modeled as TI mediums, their bulk moduli can be calculated by (King, 1964):

$$K_{TI} = \frac{C_{11}C_{33} - C_{33}C_{66} - C_{13}^2}{C_{11} - 2C_{13} + C_{33} - C_{66}} \tag{23}$$

The drained frame stiffness can be obtained while conducting the rock physics modeling in Section 3.2. If kerogen is dispersed as a type of pore-filling, the drained frame stiffness is from the DEM in the anisotropic domain (Eq. (8)). If kerogen
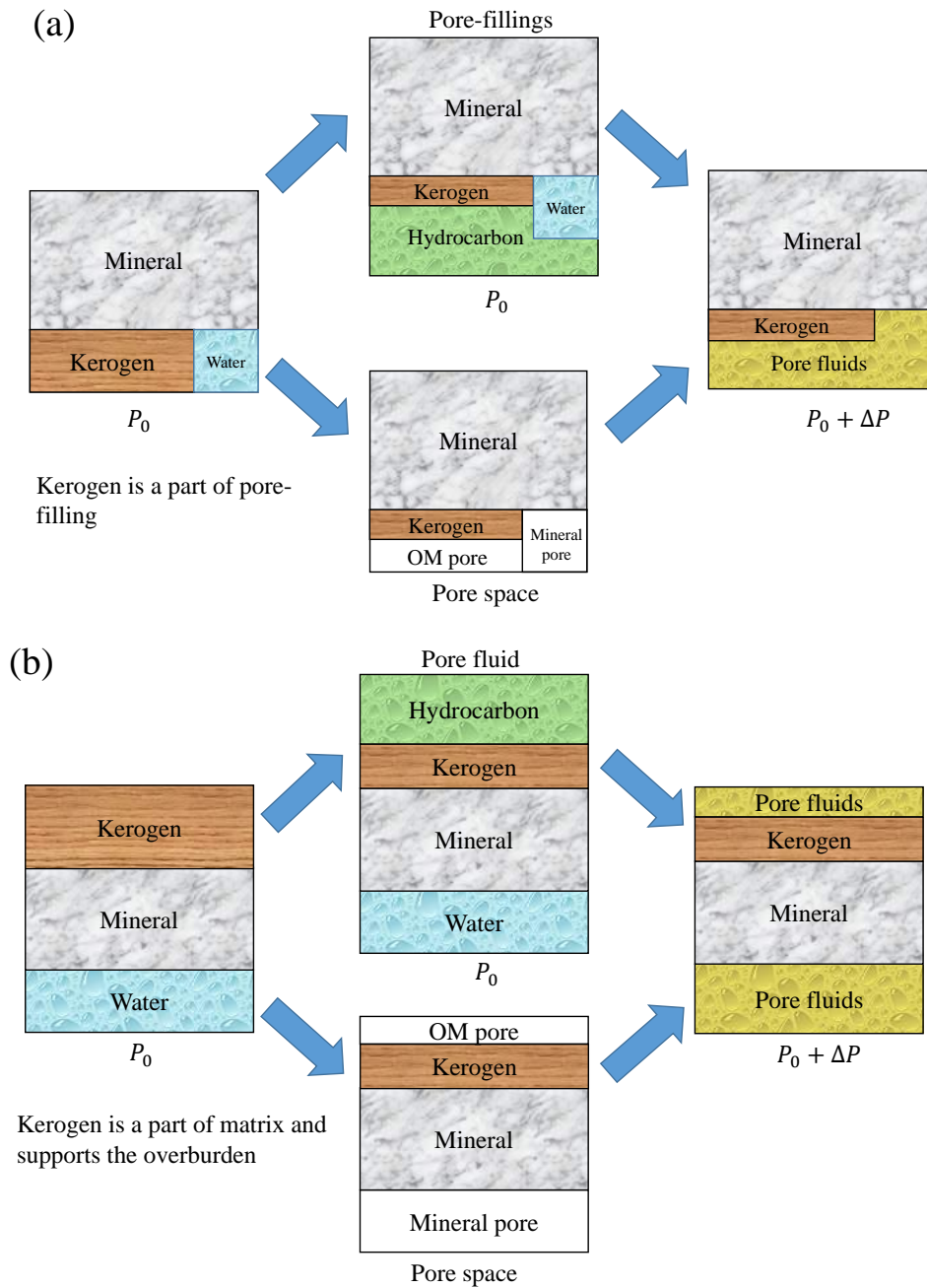
Fig. 4. The schematics of pore-filling mixture and pore space volume when (a) kerogen is a part of pore-filling and (b) kerogen is a part of matrix.

is distributed as laminae, the drained frame stiffness can be calculated by using the Backus average theory (Eq. (11)). The pore fluid modulus is set as zero when computing the stiffness of the drained frame for both the non-kerogen part and the kerogen part.

After the pore pressure increase is solved (Eqs. (16) and (21)), the porosity and density of the rock are updated according to the effective stress law. According to Berryman (1992), the relative change in porosity can be expressed as:

$$\frac{\Delta\varphi}{\varphi} = -\frac{\alpha - \varphi}{\varphi K_d}\left(\Delta Pc - \chi\Delta P\right) \tag{24}$$

where ΔPc is the change of the confining pressure, which is set a zero here; k_d is the drained matrix bulk modulus; φ is the total porosity; α is the Biot coefficient ($\alpha = 1 - K_d/K_0$), and the effective stress coefficient χ is set to unity by assuming homogeneity. With the updated porosity and density, the stiff-
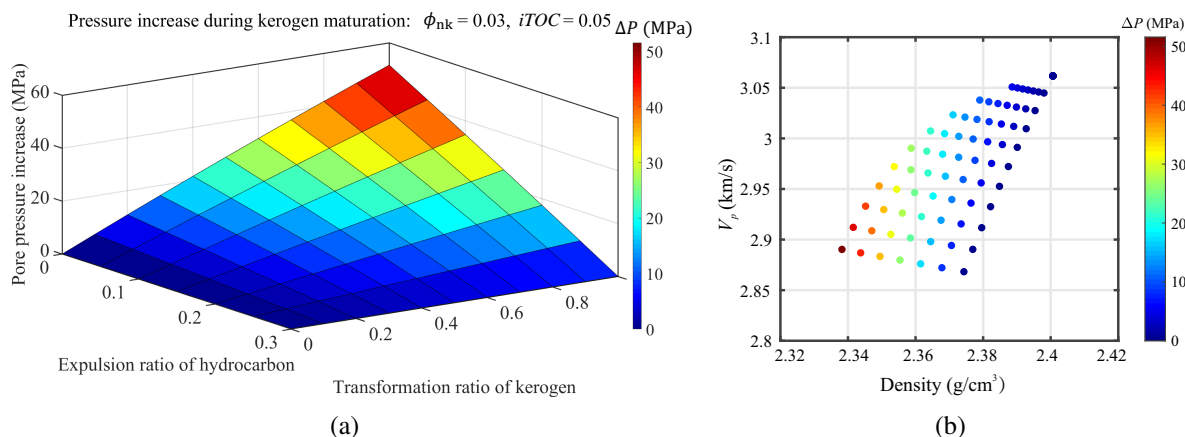
Fig. 5. The modeling results when kerogen is a part of pore-filling: (a) pore pressure increase as a function of transformation ratio of kerogen (F) and expulsion ratio of hydrocarbon (E) and (b) modeled organic shale vertical P-wave velocity (km/s) vs. density (g/cm^3) with color-coded pore pressure increase.

Table 1. Common modeling parameters of two scenarios.

Parameters	Values
Non-kerogen-related porosity (ϕ_{nk})	3%
Quartz volume fraction in the mineral mixtures	60%
Clay volume fraction in the mineral mixtures	40%
Incipient hydrogen index (HI)	400 mg HC/g TOC
Oil density (ρ_{HC})	0.84 g/cm^3
Water density	1.04 g/cm^3
Water bulk modulus (K_w)	2.5 GPa
Kerogen solid density (ρ_k)	1.2g/cm^3
Kerogen bulk modulus (K_{om})	4 GPa
Aspect ratio of clay mineral	0.05
Aspect ratio of mineral pore	0.05
Weight fraction of carbon in OM (W_k)	0.78

ness of organic shale and pore pressure increase are also updated iteratively until convergence.

It is worth mentioning that, as a theoretical model, the aim is to characterize the overpressure and seismic responses of organic shales by focusing on the primary factors. Factors dominating the overpressure generated by the hydrocarbon generation include the impacts of maturation, the volume of pore fluid contents, and the poroelastic properties of the rock. There are several factors that were not considered: 1) the main OM types at different maturity stage are different. In particular, at the overmature stage, the bitumen instead of kerogen mainly cracks into gas leading to the pore pressure increase. Therefore, the different OM types need to be distinguished in the future study. 2) the role of water during the process of maturation: oil is the main product in the experiment of hydrous pyrolysis compared to only bitumen in the anhydrous

test (Lewan and Roy, 2011). 3) Bulk volume models based on the morphology of OM were proposed. Kerogen may play a role transforming from a part of the rock matrix to a part of pore-filling due to kerogen decomposition, or kerogen plays a mixed role in shales. 4) The shape of kerogen relates to the propagating directions of hydro-fractures. For instance, vertical fractures tend to be formed in the spherical kerogen at proper stress conditions. However, horizontal fractures are found when lenticular kerogen exists. Therefore, the effects of fractures on the elastic stiffness and storage capacity can be considered during kerogen maturation. Nevertheless, after the expulsion of hydrocarbon fractures organic shale, the pore pressure soon dissipates, and fractures tend to remain closed, which exercises limited effects on the equivalent elasticity of organic shale and contributes little to the storage space. Thus, fracture effects are not our priority in this study.

4. Modeling results and analysis

According to the expressions of pore pressure increase (Eqs. (16) and (21)), the lability (N), kerogen transformation ratio (F), and hydrocarbon expulsion ratio (E) control the magnitude of overpressure if the density and compressibility of each component are irrelevant with pressure. Using a grid search method for a series of kerogen transformation ratio and hydrocarbon expulsion ratio, the excess pore pressure due to the transformation of kerogen-to-oil and the evolution of elastic properties for two scenarios are modeled: kerogen as a part of pore-filling and as a part of load-bearing role. Common modeling parameters in two scenarios are listed in Table 1, e.g., the initial non-kerogen-related porosity is 3%, quartz and clay compose the inorganic mineral phase with a volumetric fraction of 60% and 40% respectively, and the incipient TOC is 5% before maturation.

4.1 Kerogen as a part of pore-filling

In Fig. 5, the scenario is illustrated when kerogen serves as a part of pore-filling. Fig. 5(a) plots the pore pressure
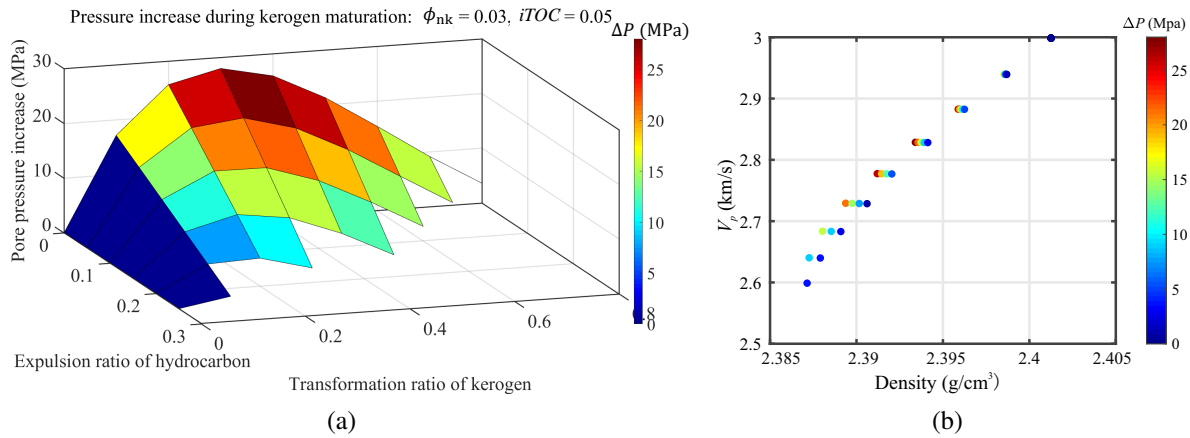
(a)   (b)

Fig. 6. The modeling results when kerogen is a part of load-bearing: (a) pore pressure increase as a function of transformation ratio of kerogen (F) and expulsion ratio of hydrocarbon (E) and (b) modeled organic shale vertical P-wave velocity (km/s) vs. density (g/cm^3) with color-coded pore pressure increase.

increase (MPa) in the Z-axis with color-code varying as a function of the transformation ratio of labile kerogen and expulsion/leakage ratio of oil. As expected, with an increasing transformed degree of kerogen, the generated pore pressure increases. Without considering a fracturing pressure, the excess pore pressure is over 50 MPa. The leakage degree of hydrocarbon has a canceling effect on the accumulation of overpressure.

In Fig. 5(b), the vertical P-wave velocity (km/s) (propagating in the direction perpendicular to the shale bedding) versus bulk density (g/cm^3) of organic shale are plotted along with the color-coded pore pressure increase. Two arrows are added to indicate how the P-wave velocity and density vary with the increases in the transformation ratio of labile kerogen and expulsion ratio of hydrocarbon. During the transformation of kerogen-to-oil, the velocity can decrease up to 7% ($\sim$0.2 km/s), and density decreases trivially (2% or 0.06 g/cm^3). The increasing degree of transformed kerogen decreases P-wave velocity because of the oil generation and decreases density because of the porosity enlarged by the increase in pore pressure. Leakage/expulsion of oil has little impact on velocity but can decrease the pore pressure and increase shale density to a small degree (less than 2%) since the light component loses. Overall, the characteristics of a decrease in velocity and a slight decrease in density along with the increase of pore pressure resemble the fluid expansion unloading model (Hoesni, 2004; Katahara, 2006; Ramdhan and Goulty, 2011).

4.2 Kerogen as a part of load-bearing

In Fig. 6, the scenario is illustrated when kerogen serves as a part of load-bearing. The incipient TOC is 5% before maturation. Similar to the first scenario, a low degree of expulsed hydrocarbon maintains high overpressure in Fig. 6(a). However, an increasing transformation ratio of kerogen first increases but then decreases the overpressure. The overpressure increases initially with the transformation ratio because the generated hydrocarbon volume is larger than the produced pore space volume at the initial stage of maturation. Two reasons

are causing the subsequent decrease in overpressure. First, the void space volume and the pore compressibility are enhanced continuously. Second, the volume difference between fluids and pore space decreases at a higher degree of transformation ratio. The former increases the denominator, and the latter decrease the numerator for the expression of the overpressure (Eq. (21)), so the overpressure is decreased. Besides, results with negative pore pressure increase are dismissed, e.g., the results generated by an expulsion ratio of hydrocarbon larger than 25%. During the transformation of kerogen-to-oil, in Fig. 6(b), the modeling vertical P-wave velocity and density decrease by $\sim$13% and $\sim$0.5%, respectively. The expulsion ratio can slightly increase density in that when the generated oil leaks or escapes, the pore pressure decreases, and so does the void porosity (sum of kerogen-related and non-kerogen-related porosities).

It is noteworthy that the first scenario has a stiffer framework than the second because of the role of kerogen. With the stiffer framework, the effective P-wave velocity is higher, and so is the peak overpressure for the first scenario. The stiff rock frame accumulates pore pressure fast because the pore space is difficult to enlarge, and the pore-fillings are severely compressed while the pore space accommodates the pore-fillings (Fig. 4).

4.3 Application on well-log data interpretation

The modeling is calibrated with the log data of a well in offshore China, where hydrocarbon generation is speculated to be responsible for the sharp increase in pore pressure within an interval of 270 m thickness. The pressure profile against depth is plotted in Fig. 7(a). Black and blue curves denote the overburden stress calculated from the density log and the hydrostatic pore pressure. The red curve is the estimated pore pressure from the mud weight and is compared with the results from the modular formation dynamics tester denoted by red asterisks. Red asterisks denote the pore pressure from the modular formation dynamics tester and calibrate the estimated pore pressure. The depth of overpressure onset is at 4,100
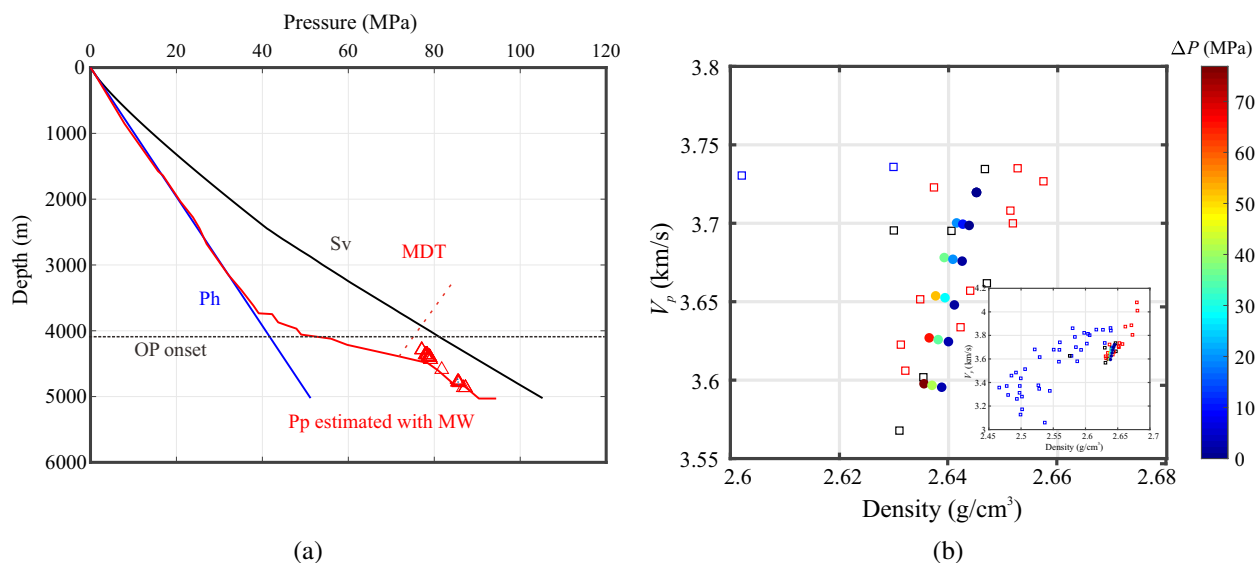
Fig. 7. (a) Pressure profile (MPa) varying with depth (m) for a well and (b) application of interpreting well log data with the proposed model. The vertical well includes a zone with a quick increase in pore pressure. The modeled velocity and density are plotted with the filled circles with the color-coded pore pressure increase.

m according to the logging run and marked with the black dashed line. In Fig. 7(b), the averaged velocity and density data are plotted using the Backus average on each 40 m depth interval near the pressure transition zone, and the inset to the bottom right shows the complete V_p-density data upscaled from the entire well log data. The upscaled log data enables us to investigate the whole trend without the interference of high-frequency fluctuations. The data denoted by blue, black, and red squares represent data with respective depths ranging from less than 4,100 m, between 4,100 and 4,370 m, and greater than 4,370 m. The data in the shallow section shows a trend of velocity and density (blue squares) increasing with depth. Within the intermediate section, velocity and density deflect with the NCT, and the data trend moves approximately downward with depth. Within the pressure transition zone (black squares), the pore pressure is quickly built up, and the P-wave velocity and density reduce ~7% (0.2 km/s) and ~1% (0.02 g/cm^3) respectively. With the increasing depth in the deep section, the V_p and density data (red squares) both increase and move toward the extrapolation of the NCT, and the pore pressure increases at a rate lower than within the pressure transition zone. Tingay et al. (2013) report a similar pattern for the overpressure generated by the thermal maturation in the Malay Basin.

The sharp increase in pore pressure within the pressure transition zone cannot be characterized by the conventional empirical method. To interpret how the elasticity and pore pressure vary within the transition zone, the modeling results are plotted with color-coded filled circles to compare with the target data (black squares). Some modeling inputs are listed as follows: the mineral porosity of 1% and the incipient TOC of 2% are averaged from the well log data of the transition zone. Illite is assumed to be the primary clay mineral since the depths of interest are relatively deep (> 4,000 m), and the

bulk density is relatively high (> 2.63 g/cm^3). The organic phase is treated as a part-of pore filling because of the small volume fraction of soft component (porosity and TOC) and the relatively rigid framework. Two data points in black squares move rightward and are out of the range predicted by the modeling, which might be caused by the heterogeneity of the composition. The model captures the downward data trend of the transition zone. The modeling results suggest a fast build-up in pore pressure for organic shale zones with a decrease in velocity and a slight decrease in density. Though sonic velocity and density vary to some extent, the limited void space (small mineral pore and OM pore constrained by the low TOC content) accounts for the rapid pore pressure increase.

5. Discussion

5.1 Modeling results when om pore can be compacted

In the modeling scheme, it is assumed that the kerogen-related porosity is related to the transformation or maturation degree of kerogen (Eq. (4)). In general, there are two typical phases of kerogen, dispersed spheroids or continuous laminae. The OM pores are easier to remain open in the kerogen as a part of pore-filling than as a part of load-bearing. For instance, the larger organic domains in a laminar shape are non-porous in Fig. 1(b), which may have been compacted in situ. Therefore, the scenario when OM pore can be plastically compacted is considered, and its impact on the modeling results is discussed.

There is a trade-off between mechanical compaction and thermal maturation controlling the porosity variation trend with depth. In Milliken et al. (2012), based o the core samples data from two wells, they found that when the TOC content is relatively low, the porosity in data from both wells increases
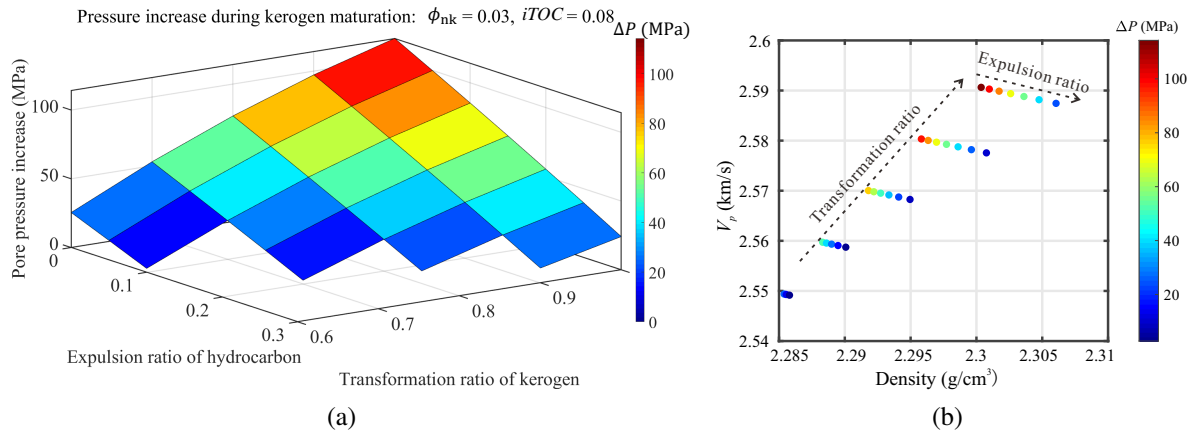
Fig. 8. The modeling results when kerogen is a part of matrix, and OM pore can be compacted plastically: (a) pore pressure increase as a function of transformation ratio of kerogen (F) and expulsion ratio of hydrocarbon (E) and (b) modeled organic shale vertical P-wave velocity (km/s) vs. density (g/cm^3) with color-coded pore pressure increase.

with the TOC content, which is consistent with the relationship between OM-related porosity and organic richness in Eq. (4). Such a linear relationship also accords with the modeling result of shale samples in the Powder River Basin of Wyoming (Modica and Lapierre, 2012). By contrast, when TOC is relatively high, the linear trend deflects, suggesting the effect of overburden that decreases pore space cancels the impact of maturation that increases pore space. A similar pattern can also be observed from various unconventional shale samples by Sone and Zoback (2013). Moreover, Sone and Zoback (2013) indicates samples with high organic richness happen to contain higher clay content than samples with low organic richness, so kerogen tends to form a continuous network in the clay-rich samples shown in Fig. 1(b).

Thus, when OM is a part of load-bearing, and the TOC is relatively abundant, the generated void space within kerogen tends to be more compacted and does not change much with TOC. A constant, e.g., 4%, is attributed to the kerogen-related porosity (ϕ_k). As organic shale is compacted during kerogen maturation, the bulk volume keeps decreasing and can be expressed as:

$$V_T = \frac{1 - NFK_i(1 - \phi_{n0})}{1 - \phi_k} \qquad (25)$$

The non-kerogen-related porosity is updated through:

$$\phi_{n2} = \frac{\phi_{n0}}{V_T} \qquad (26)$$

where ϕ_{n0} denotes the initial non-kerogen-related porosity at 3%; ϕ_{n2} denotes the non-kerogen-related porosity after updating. By substituting the updated bulk volume (Eq. (25)) into the volume fractions of minerals and solid OM (Eqs. (5) and (6)), and the volumes of void space, solid OM, and initial water (Eqs. (18)-(20)), the parameters for modeling are updated. The modeling results can be updated when OM is a part of load-bearing.

The initial TOC is set to 8% before maturation. Similar to the scenario that kerogen serves as a part of pore-filling, a high degree of transformed kerogen and a low degree of expulsed

hydrocarbon yield high overpressure in Fig. 8(a). The peak overpressure is above 110 MPa without considering a fracturing pressure. The peak overpressure is enhanced because OM pore can be compacted. The framework becomes stiffer than the scenario that OM pore cannot be compacted plastically. Some yielded pore pressure increase through Eq. (16) are negative and therefore omitted, e.g., the results generated by a low transformation ratio of kerogen and a high expulsion ratio of hydrocarbon. During the transformation of kerogen-to-oil, Fig. 8(b) suggests that the vertical P-wave velocity and density increase trivially by ~1.5% and ~1% respectively. The rock becomes stiffer because the OM pores are compacted, and the volume fraction of soft components decreases. The expulsion ratio of oil has smaller impacts on velocity and density than the transformation ratio of labile kerogen.

5.2 Elastic characteristics compared with other overpressure mechanisms

The proposed modeling framework demonstrates the evolution of elastic characteristics and overpressure due to thermal maturation for various scenarios. Signatures of overpressure generated by thermal maturation and some other common mechanism are sketched in Fig. 9. For instance, the velocity and density increase with depth under normal compaction. Velocity and density data become concentrated near the NCT if the disequilibrium compaction occurs. If there is no plastic compaction during the hydrocarbon generation, P-wave velocity decreases, and density decreases trivially for both the scenarios of kerogen acting as pore-filling and load-bearing role. Its data trend resembles the signature of pure fluid expansion during the process of smectite-to-illite transition (Hoesni, 2004; Qin et al., 2019). No matter whether the yielded hydrocarbon seldom or partially escapes or migrates, the data trend of organic shale moves mainly downward. By contrast, if released water during the smectite-to-illite transition can escape partly or entirely, the density can increase and leave a rightward trend, as shown in Fig. 9. The primary reason why signatures of the two overpressure mechanisms differ is the
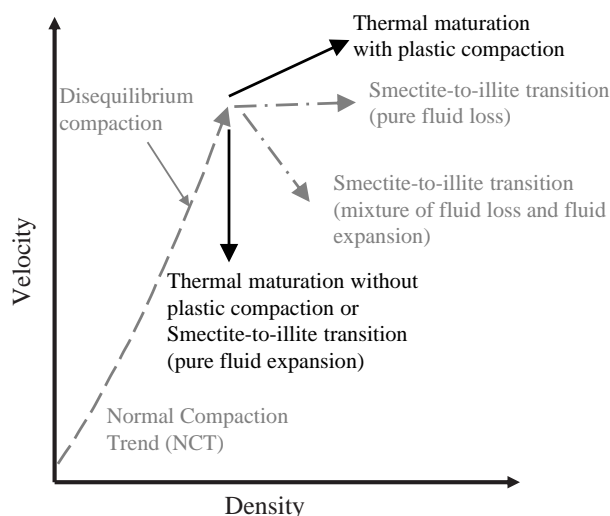
Fig. 9. Sketch of signatures for several shale overpressure mechanisms on velocity-density profile, e.g., disequilibrium compaction, thermal maturation, and smectite-to-illite transition.

component's density contrast before or after the phase change, i.e., the density ratio of organic solid or kerogen to hydrocarbon is higher than the ratio of clay interlayer water to free water. If the plastic compaction occurs, the sonic velocity and density of organic shale both can increase a little, as shown in Fig. 9, resulting from the decrease in the volume fraction of soft components.

6. Conclusions

A framework is proposed to model elastic signatures of overpressure in organic shales based on the characterization of the pore pressure evolution processes due to thermal maturation. Main considerations include the morphology of kerogen and its role in organic shales. Different bulk volume models for these shales are suggested. Kerogen, due to its dispersed distribution and spherical shape, is seen as part of the pore-filling component. It also takes on a load-bearing role because of its continuous network and layered structure. Different schemes are then crafted to mimic the equivalent elasticity of organic shales and gauge the overpressure based on thermal maturation and hydrocarbon expulsion. The outcomes from this modeling lead to specific conclusions:

1) The volume ratio of pore water to the initial kerogen determines the maximum overpressure no matter whether kerogen serves as a part of pore-filling or load-bearing. If kerogen is a part of pore-filling, an increase in the transformation degree of kerogen or a decrease in the expulsion degree of hydrocarbon helps to increase the pore pressure due to the maturation or transformation of kerogen. If kerogen is a part of load-bearing, an increase in the transformation degree of kerogen first increases but then decreases the overpressure. The bulk volume model considers the case without plastic compaction for the OM pore created due to the thermal maturation and causes the non-monotonic characteristic of overpressure.

2) If the OM pore cannot be compacted plastically, the

modeled elastic property variation resembles the fluid expansion unloading model, i.e., velocity decreases and density changes little when pore pressure increases. The V_p/V_s ratios are sensitive to the transformation degree of kerogen compared to the expulsion degree of hydrocarbon. If kerogen serves as a part of pore-filling, V_p/V_s ratios can slightly decrease due to the maturation. If kerogen serves as a part of load-bearing, V_p/V_s ratios can increase to a certain degree.

3) If the OM pore can be compacted plastically, the maximum overpressure is higher than the case when the OM pore cannot be compacted plastically. Overpressure rises because the storage space of organic shales decreases. Due to the behavior of the continual compaction, P-wave velocity and density of organic shales increase trivially due to the overpressure caused by the thermal maturation.

Acknowledgements

Conflict of interest

The authors declare no competing interest.

References

Alfred, D., Vernik, L. A new petrophysical model for organic-rich shales. Paper SPWLA-2017-217 Presented at the SPWLA 53rd Annual Logging Symposium, Cartagena, Colombia, 16-20 June, 2012.

Backus, G. E. Long-wave elastic anisotropy produced by horizontal layering. Journal of Geophysical Research, 1962, 67(11): 4427-4440.

Barker, C. Calculated volume and pressure changes during the thermal cracking of oil to gas in reservoirs. AAPG Bulletin, 1990, 74(8): 1254-1261.

Berg, R. R., Gangi, A. F. Primary migration by oil-generation microfracturing in low-permeability source rocks: Application to the Austin Chalk, Texas. AAPG Bulletin, 1999, 83(5): 727-756.

Berryman, J. G. Long-wavelength propagation in composite elastic media I. Spherical inclusions. The Journal of the Acoustical Society of America, 1980, 68(6): 1809-1819.

Berryman, J. G. Effective stress for transport properties of inhomogeneous porous rock. Journal of Geophysical Research: Solid Earth, 1992, 97(B12): 17409-17424.

Bowers, G. L. Pore pressure estimation from velocity data: Accounting for overpressure mechanisms besides under-compaction. SPE Drilling & Completion, 1995, 10(2): 89-95.

Bruce, C. H. Smectite dehydration—its relation to structural

development and hydrocarbon accumulation in northern Gulf of Mexico basin. AAPG Bulletin, 1984, 68(6): 673-683.

Burrus, J., Osadetz, K., Wolf, S., et al. A two-dimensional regional basin model of Williston Basin hydrocarbon systems. AAPG Bulletin, 1996, 80(2): 265-290.

Cander, H. Sweet spots in shale gas and liquids plays: Prediction of fluid composition and reservoir pressure. Paper Presented at AAPG Annual Convention and Exhibition, Long Beach, California, 22-25 April, 2012.

Carcione, J. M., Gangi, A. F. Gas generation and overpressure: Effects on seismic attributes. Geophysics, 2000, 65(6): 1769-1779.

Carcione, J. M., Helle, H. B., Avseth, P. Source-rock seismic-velocity models: Gassmann versus Backus. Geophysics, 2011, 76(5): N37-N45.

Chatterjee, R., Mukhopadhyay, M., Paul, S. Overpressure zone under the Krishna-Godavari offshore basin: Geophysical implications for natural hazard in deeper-water drilling. Natural Hazards, 2011, 57: 121-132.

Chen, J., Xiao, X. Evolution of nanoporosity in organic-rich shales during thermal maturation. Fuel, 2014, 129: 173-181.

Ciz, R., Shapiro, S. A. Generalization of Gassmann equations for porous media saturated with a solid material. Geophysics, 2007, 72(6): A75-A79.

Couzens-Schultz, B. A., Axon, A., Azbel, K., et al. Pore pressure prediction in unconventional resources. Paper IPTC 16849 Presented at the International Petroleum Technology Conference, Beijing, China, 26-28 March, 2013.

Daly, A. R., Edman, J. D. Loss of organic carbon from source rocks during thermal maturation. Paper Presented at the 1987 AAPG Annual Convent Exhibition, Los Angeles, California, 7-10 June, 1987.

Dasgupta, S., Chatterjee, R., Mohanty, S. P. Magnitude, mechanisms, and prediction of abnormal pore pressure using well data in the Krishna-Godavari Basin, east coast of India. AAPG Bulletin, 2016, 100(12): 1833-1855.

Domenico, S. N. Effect of brine-gas mixture on velocity in an unconsolidated sand reservoir. Geophysics, 1976, 41(5): 882-894.

Dong, T., Harris, N. B., McMillan, J. M., et al. A model for porosity evolution in shale reservoirs: An example from the Upper Devonian Duvernay Formation, Western Canada Sedimentary Basin. AAPG Bulletin, 2019, 103(5): 1017-1044.

Eaton, B. A. The equation for geopressure prediction from well logs. Paper SPE 5544 Presented at the Fall Meetings of the Society of Petroleum Engineers of Aime, Dallas, Texas, 28 September-1 October, 1975.

Green, S., Loeffler, J., Clarke, S., et al. Using traditional methods to predict pore pressure in Devonian black shale basins of North East British Columbia. Paper URTEC 2904084 Presented at the SPE/AAPG/SEG Unconventional Resources Technology Conference, Houston, Texas, 23-25 July, 2018.

Guo, Z., Li, X., Liu, C., et al. A shale rock physics model for

analysis of brittleness index, mineralogy and porosity in the Barnett Shale. Journal of Geophysics and Engineering, 2013, 10(2): 025006.

Gutierrez, M. A., Braunsdor, N. R., Couzens, B. A. Calibration and ranking of pore-pressure prediction models. The Leading Edge, 2006, 25(12): 1516-1523.

Hao, F., Zou, H., Gong, Z., et al. Hierarchies of overpressure retardation of organic matter maturation: Case studies from petroleum basins in China. AAPG Bulletin, 2007, 91(10): 1467-1498.

Hart, B. S., Flemings, P. B., Deshpande, A. Porosity and pressure: Role of compaction disequilibrium in the development of geopressures in a Gulf Coast Pleistocene basin. Geology, 1995, 23(1): 45-48.

Hart, B. S., Macquaker, J. H. S., Taylor, K. G. Mudstone ("shale") depositional and diagenetic processes: Implications for seismic analyses of source-rock reservoirs. Interpretation, 2013, 1(1): B7-B26.

Hauser, M. R., Petitclerc, T., Braunsdorf, N. R., et al. Pressure prediction implications of a Miocene pressure regression. The Leading Edge, 2013, 32(1): 100-109.

Hoesni, M. J. Origins of overpressure in the Malay Basin and its influence on petroleum systems. Durham, Durham University, 2004.

Hornby, B. E., Schwartz, L. M., Hudson, J. A. Anisotropic effective-medium modeling of the elastic properties of shales. Geophysics, 1994, 59(10): 1570-1583.

Jarvie, D. M., Hill, R. J., Ruble, T. E., et al. Unconventional shale-gas systems: The Mississippian Barnett Shale of north-central Texas as one model for thermogenic shale-gas assessment. AAPG Bulletin, 2007, 91(4): 475-499.

Karthikeyan, G., Kumar, A., Shrivastava, A., et al. Overpressure estimation and productivity analysis for a Marcellus Shale gas reservoir, southwest Pennsylvania: A case study. The Leading Edge, 2018, 37(5): 344-349.

Katahara, K. Overpressure and shale properties: Stress unloading or smectite-illite transformation? Paper SEG-2006-1520 Presented at the 2006 SEG International Exposition and Annual Meeting, New Orleans, Louisiana, 1-6 October, 2006.

King, M. S. Wave velocities and dynamic elastic moduli of sedimentary rocks. Berkeley, University of California, 1964.

Lash, G. G., Engelder, T. An analysis of horizontal micro-cracking during catagenesis: Example from the Catskill delta complex. AAPG Bulletin, 2005, 89(11): 1433-1449.

Lewan, M. D., Roy, S. Role of water in hydrocarbon generation from Type-I kerogen in Mahogany oil shale of the Green River Formation. Organic Geochemistry, 2011, 42(1): 31-41.

Löhr, S. C., Baruch, E. T., Hall, P. A., et al. Is organic pore development in gas shales influenced by the primary porosity and structure of thermally immature organic matter? Organic Geochemistry, 2015, 87: 119-132.

Loucks, R. G., Reed, R. M., Ruppel, S. C., et al. Morphology, genesis, and distribution of nanometer-scale pores in siliceous mudstones of the Mississippian Barnett Shale. Journal of Sedimentary Research, 2009, 79(12): 848-861.

Qin, X., et al. Advances in Geo-Energy Research, 2023, 10(3): 174-188

187

Lucier, A. M., Hofmann, R., Bryndzia, L. T. Evaluation of variable gas saturation on acoustic log data from the Haynesville Shale gas play, NW Louisiana, USA. The leading edge, 2011, 30(3): 300-311.

Luo, X., Vasseur, G. Geopressuring mechanism of organic matter cracking: Numerical modeling. AAPG Bulletin, 1996, 80(6): 856-873.

Mavko, G., Mukerji, T., Dvorkin, J. The Rock Physics Handbook. Cambridge, UK, Cambridge University Press, 2009.

Meissner, F. F. Petroleum geology of the Bakken formation Williston basin, North Dakota and Montana, in the Petroleum Geochemistry and Basin Evaluation, edited by G. Demaison and R. J. Murris, Tulsa, Oklahoma, pp. 159-179, 1978.

Milliken, K. L., Esch, W. L., Reed, R. M., et al. Grain assemblages and strong diagenetic overprinting in siliceous mudrocks, Barnett Shale (Mississippian), Fort Worth Basin, Texas. AAPG Bulletin, 2012, 96(8): 1553-1578.

Milliken, K. L., Rudnicki, M., Awwiller, D. N., et al. Organic matter–hosted pore system, Marcellus formation (Devonian), Pennsylvania. AAPG Bulletin, 2013, 97(2): 177-200.

Modica, C. J., Lapierre, S. G. Estimation of kerogen porosity in source rocks as a function of thermal transformation: Example from the Mowry Shale in the Powder River Basin of Wyoming. AAPG Bulletin, 2012, 96(1): 87-108.

Morley, C. K. Hydrocarbon generation-a possible cause of elevated pore pressures in the Osen-Roa thrust sheet, Norway. Journal of Structural Geology, 1992, 14(6): 743-747.

Mura, T. Micromechanics of Defects in Solid. Leiden, Netherlands, Martinus Nijhoff Publishers, 1987.

Nishizawa, O. Seismic velocity anisotropy in a medium containing oriented cracks transversely isotropic case. Journal of Physics of the Earth, 1982, 30(4): 331-347.

Nur, A., Mavko, G., Dvorkin, J., et al. Critical porosity: A key to relating physical properties to porosity in rocks. The Leading Edge, 1998, 17(3): 357-362.

Passey, Q. R., Bohacs, K. M., Esch, W. L, et al. From oil-prone source rock to gas-producing shale reservoir–geologic and petrophysical characterization of unconventional shale-gas reservoirs. Paper SPE 131350 Presented at the International Oil and Gas Conference and Exhibition in China, Beijing, China, 8-10 June, 2010.

Passey, Q. R., Creaney, S., Kulla, J. B., et al. A practical model for organic richness from porosity and resistivity logs. AAPG Bulletin, 1990, 74(12): 1777-1794.

Qin, X., Han, D., Zhao, L. Rock physics modeling of organic-rich shales with different maturity levels. Paper SEG-2014-1584 Presented at the 2014 SEG Annual Meeting, Denver, Colorado, USA, 26-31 October, 2014.

Qin, X., Han, D., Zhao, L. Elastic characteristics of overpressure due to smectite-to-illite transition based on micromechanism analysis. Geophysics, 2019, 84(4): WA23-WA42.

Qin, X., Zhao, L., Cai, Z., et al. Compressional and shear wave velocities relationship in anisotropic organic shales.

Journal of Petroleum Science and Engineering, 2022, 219: 111070.

Ramdhan, A. M., Goulty, N. R. Overpressure and mudrock compaction in the Lower Kutai Basin, Indonesia: A radical reappraisal. AAPG Bulletin, 2011, 95(10): 1725-1744.

Sayers, C. M. The elastic anisotrophy of shales. Journal of Geophysical Research: Solid Earth, 1994, 99(B1): 767-774.

Sayers, C. M. An introduction to velocity-based pore-pressure estimation. The Leading Edge, 2006, 25(12): 1496-1500.

Sayers, C. M. The effect of anisotropy on the Young's moduli and Poisson's ratios of shales. Geophysical Prospecting, 2012, 61(2): 416-426.

Seewald, J. S. Organic–inorganic interactions in petroleum-producing sedimentary basins. Nature, 2003, 426(6964): 327-333.

Sone, H., Zoback, M. D. Mechanical properties of shale-gas reservoir rocks—Part 1: Static and dynamic elastic properties and anisotropy. Geophysics, 2013, 78(5): D381-D392.

Swarbrick, R. E., Osborne, M. J. Mechanisms that generate abnormal pressures: An overview, in The Abnormal Pressures in Hydrocarbon Environments, edited by B. E. Law, G. F. Ulmishek and V. I. Slavin, Tulsa, Oklahoma, pp. 13-34, 1998.

Swarbrick, R. E., Osborne, M. J., Yardley, G. S. Comparison of overpressure magnitude resulting from the main generating mechanisms, in The Pressure Regimes in Sedimentary Basins and Their Prediction, edited by A. R. Huffman and G. L. Bowers, Tulsa, Oklahoma, pp. 1-12, 2001.

Tingay, M. R. P., Morley, C. K., Laird, A., et al. Evidence for overpressure generation by kerogen-to-gas maturation in the northern Malay Basin. AAPG Bulletin, 2013, 97(4): 639-672.

Tissot, B. P., Pelet, R., Ungerer, P. H. Thermal history of sedimentary basins, maturation indices, and kinetics of oil and gas generation. AAPG Bulletin, 1987, 71(12): 1445-1466.

Tosaya, C. A. Acoustical properties of clay-bearing rocks. Palo Alto, Stanford University, 1982.

Vanorio, T., Mukerji, T., Mavko, G. Emerging methodologies to characterize the rock physics properties of organic-rich shales. The Leading Edge, 2008, 27(6): 780-787.

Vernik, L. Hydrocarbon-generation-induced microcracking of source rocks. Geophysics, 1994, 59(4): 555-563.

Vernik, L., Landis, C. Elastic anisotropy of source rocks: Implications for hydrocarbon generation and primary Migration1. AAPG Bulletin, 1996, 80(4): 531-544.

Vernik, L., Milovac, J. Rock physics of organic shales. The Leading Edge, 2011, 30(3): 318-323.

Walls, J. D., Diaz, E. Relationship of shale porosity permeability trends to pore type and organic content. Denver Well Logging Society, Petrophysics in Tight Oil Workshop, 2011.

Yan, F., Han, D. Measurement of elastic properties of kerogen. Paper SEG 2013 1319 Presented at the 2013 SEG Annual

Meeting, Houston, Texas, 22-27 September, 2013.

Yang, Y., Mavko, G. Mathematical modeling of microcrack growth in source rock during kerogen thermal maturation. AAPG Bulletin, 2018, 102(12): 2519-2535.

Yu, H. Dynamic effective pressure coefficient calibration. Geophysics, 2015, 80(1): D65-D73.

Zhang, J. Pore pressure prediction from well logs: Methods, modifications, and new approaches. Earth-Science Reviews, 2011, 108(1-2): 50-63.

Zhang, H., Yin, X., Li, K., et al. Estimation of effective stress parameters in fractured reservoirs based on 5D seismic data. Geophysical Prospecting for Petroleum, 2022, 61(3): 521-542. (in Chinese)

Zhao, L., Cai, Z., Qin, X., et al. An empirical elastic anisotropy prediction model in self-sourced reservoir shales and its influencing factor analysis. Geophysics,

2023, 88(3): MR117-MR126.

Zhao, L., Qin, X., Han, D., et al. Rock-physics modeling for the elastic properties of organic shale at different maturity stages. Geophysics, 2016, 81(5): D527-D541.

Zhao, L., Qin, X., Zhang, J., et al. An effective reservoir parameter for seismic characterization of organic shale reservoir. Surveys in Geophysics, 2018, 39: 509-541.

Zhu, Y., Xu, S., Payne, M., et al. Improved rock-physics model for shale gas reservoirs. Paper SEG-2012-0927 Presented at the 2012 SEG Annual Meeting, Las Vegas, Nevada, 4-9 November, 2012.

Zimmerman, R. W. Compressibility of Sandstones. Amsterdam, Netherland, Elsevier, 1991.

Zou, C., Ding, Y., Lu, Y., et al. Concept, technology and practice of "man-made reservoirs" development. Petroleum Exploration and Development, 2017, 44(1): 146-158.